Control-Loop Design for Nonlinear Sensors (AASERT) Final Report

Thomas B. Gabrielson
Applied Research Laboratory
The Pennsylvania State University
P.O. Box 30
State College, PA 16804
tbg3@psu.edu

Contract N00014-97-1-0676
Program Officer: Dr. Roy Elswick
ONR 321SS
Office of Naval Research
Ballston Centre Tower One
800 North Quincy Street
Arlington, VA 22217-5660

7 September, 2000

ABSTRACT

While linear control theory is well developed, the practice of restricting systems to operate solely in linear regions can seriously limit the achievable performance. New technologies and new applications would be enabled by better understanding of the closed-loop control of nonlinear systems. If robust control loops can be designed in the presence of these nonlinearities and points of instability, the performance of these systems can be enhanced significantly. For example, controlled operation in or near regions of inherent instability can result in improved bandwidth, response time, and a wider envelope of operation.

REPORT DOCUMENTATION PAGE

Form Approved
OMB No. 0704-0188

1. AGENCY USE ONLY *(Leave Blank)*	2. REPORT DATE	3. REPORT TYPE AND DATES COVERED
	7 September 2000	Final 01 June 1997 - 30 June 2000

4. TITLE AND SUBTITLE
Control-Loop Design for Nonlinear Sensors

5. FUNDING NUMBERS
G: N00014-97-1-0676
PR: 97PR05713-00

6. AUTHORS
Thomas B. Gabrielson

7. PERFORMING ORGANIZATION NAME(S) AND ADDRESS(ES)
The Pennsylvania State University
Office of Sponsored Programs
110 Technology Center Building
University Park, PA 16802-7000

8. PERFORMING ORGANIZATION REPORT NUMBER
FD-321-00-02

9. SPONSORING / MONITORING AGENCY NAME(S) AND ADDRESS(ES)
Office of Naval Research (ONR 252: Diane Gales)
Balston Centre Tower One
800 North Quincy Street
Arlington, VA 22217-5560

10. SPONSORING / MONITORING AGENCY REPORT NUMBER

11. SUPPLEMENTARY NOTES

12a. DISTRIBUTION / AVAILABILITY STATEMENT
Approved for Public Release; Distribution is Unlimited

12b. DISTRIBUTION CODE

13. ABSTRACT *(Maximum 200 words)*

While linear control theory is well developed, the practice of restricting systems to operate solely in linear regions can seriously limit the achievable performance. New technologies and new applications would be enabled by better understanding of the closed-loop control of nonlinear systems. If robust control loops can be designed in the presence of these nonlinearities and points of instability, the performance of these systems can be enhanced significantly. For example, controlled operation in or near regions of inherent instability can result in improved bandwidth, response time, and a wider envelope of operation.

14. SUBJECT TERMS
Acoustics, USW, Closed-Loop Control, Feedback, Electron Tunneling, Accelerometer

15. NUMBER OF PAGES
20

16. PRICE CODE

17. SECURITY CLASSIFICATION OF REPORT	18. SECURITY CLASSIFICATION OF THIS PAGE	19. SECURITY CLASSIFICATION OF ABSTRACT	20. LIMITATION OF ABSTRACT
U	U	U	UL

INTRODUCTION

Many advanced-concept sensors and control systems are nonlinear and some operate in or near inherent instabilities. While linear control theory is well developed, the practice of restricting systems to operate solely in linear regions can seriously limit the achievable performance. New technologies and new applications would be enabled by better understanding of the closed-loop control of nonlinear systems.

The initial focus of this project was a directional acoustic sensor based on electron tunneling. This device exploits the nonlinear quantum tunneling function to produce exceptionally high-sensitivity. The relationship of the quantum-mechanical tunneling current to displacement is the product of an exponential function of the displacement and the reciprocal of the displacement[1], while the electrostatic closed-loop control structure produces a force that varies as the square of the control voltage. Consequently, this system is strongly nonlinear for large-displacement perturbations and reaches instability ("snap down") for moderate electrostatic deflections.

Expensive and complex linearizing circuitry[2] is sometimes used in electron-tunneling devices; however, experience with the subject device has shown that this is not necessary in some applications[3]. If robust control loops can be designed in the presence of these nonlinearities and points of instability, the performance of these electron-tunneling sensors can be enhanced significantly[4]. For example, controlled operation in or near regions of inherent instability[5] can result in improved bandwidth, response time, and a wider envelope of operation[6].

As the parent project evolved, fabrication of the electron-tunneling transducer proved to be problematic so a differential-capacitance transducer was used instead. The impact on the AASERT project was small since the closed-loop control of the differential-capacitance device presents similar challenges: both the electrostatic actuation and the damping are nonlinear and the potential still exists for large-amplitude instability.

This AASERT project consisted of two essential components:

- development of a design model for nonlinear, potentially unstable systems like the closed-loop differential-capacitance sensor, and
- demonstration of various aspects of noise and control on a series of electromechanical structures.

The design model was implemented in Simulink and MatLab[7]. The demonstrations of various aspects of system behavior were implemented as a graded series of laboratory experiments to provide graduate students with a more substantial foundation in nonlinear control.

RESEARCH ACTIVITIES

The parent project provided the context for these control-loop investigations. Development of the electron-tunneling transducer raised the issue of control-loop stability for large-amplitude motion. These transducers were often stable for small-amplitude motion but, if strongly excited, could start large-amplitude oscillation. The desirability of closed-loop operation for improved frequency response or dynamic range made understanding of these large-amplitude effects important. While the differential-capacitance accelerometer is not as strongly nonlinear in sensing, it does have inherently nonlinear actuation and damping so the modeling effort remained focused on analysis of nonlinear closed-loop systems for large-amplitude motion.

Development of a personal-computer-based model

The student developed a model for coupled electrical and mechanical structures including large-displacement electrostatic actuators, electron-tunnel gaps, nonlinear springs, electrodynamic actuators, and piezoelectric actuators. Adaptation of existing electric-circuit simulation models (like SPICE) were considered first, but it was eventually decided to develop a suitable model from first principles. The performance of that model was verified with small-displacement linear systems.

Construction of test structures

The student built several for use in validating nonlinear aspects of the control model. These structures were:

- a strongly nonlinear spring system,
- an inverted pendulum with both stable and unstable operation, and
- a capacitive sensor with electrodynamic actuation.

These structures formed the basis for several laboratory experiments for a graduate course in sensors and control.

PRODUCTS

The AASERT research produced the following:

- A PC-based model for design and performance prediction of nonlinear control-loop structures.

- A demonstration apparatus for illustrating the following aspects of a control system: (a) spring nonlinearity, (b) inverted-pendulum instability, (c) loop instability.

- Five teaching modules (hardware, lecture notes, and laboratory instructions) for illustration of various aspects of sensing and control.

Detailed descriptions of these products can be found in the sections below. The next section describes the state-variable model for nonlinear control-loop architecture. The section after that describes the five laboratory experiments that were developed.

STATE-VARIABLE MODEL FOR CLOSED-LOOP ACCELEROMETERS[8]

The goal of this phase of the research was to develop a model for simulation and analysis of feedback for nonlinear control systems. In the design of high-performance, miniature accelerometers, it is possible to improve performance by adding feedback. Feedback can be used to improve linearity, bandwidth, dynamic range, and noise performance. However, these improvements cannot, in general, be realized simultaneously. The addition of feedback involves tradeoffs between various performance enhancements and it is important to be able to analyze these tradeoffs before building hardware.

The principal focus was to develop a general-purpose model for feedback simulation that is capable of evaluating both small- and large-deflection dynamics. This necessarily includes nonlinear effects with regard to practical sensing and actuation techniques. Both electrostatic actuation and electron-tunneling detection are nonlinear and, while systems can be stable for small oscillations, large-amplitude instabilities can ruin the performance of a high-sensitivity system.

Objectives of Feedback Control

Application of feedback to a sensor system typically involves the addition of an actuator. Part of the sensed signal is amplified and applied to the actuator according to some control strategy. The actuation may be applied to restrict the motion of the proof mass, for example. If the control force is sufficient to counter the input excitation so that the proof-mass motion is small, then an inherently nonlinear restoring force (for example) can be treated as linear. This not only produces linear output, it can also greatly increase the sensor's dynamic range.

Furthermore, a sensor's open-loop dynamic response usually includes a mechanical resonance. The frequency of that resonance affects the response and the sensor design must consider this. The normal open-loop strategy is to design the resonance to be well above the band of interest; however, this can lead to other compromises. If the resonance is moved into the band of interest, then feedback can be applied to flatten the response through and beyond the natural resonance.

If a very-low self-noise is required, a high-Q mechanical design might be used. This reduces the level of intrinsic thermal-agitation noise in the mechanical system but the high Q can cause problems in transient response or dynamic range. Again, feedback can be applied to flatten the response through the resonance and reduce these problems.

However, these objectives cannot all be addressed successfully in a single implementation. Increasing linearity may raise the self-noise level; increasing the bandwidth may reduce the dynamic range.

Simple Feedback Example

To illustrate these tradeoffs and to set the stage for introduction of the state-variable technique, consider the simple feedback system shown in Fig. 1.

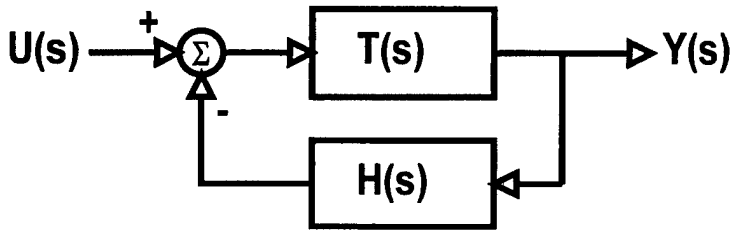

Figure 1. Simple feedback system with input, *U*, and output, *Y*. The open-loop transfer function is *T* and the feedback transfer function is *H*.

The open-loop transfer function, T_{ol}, in the *s*-domain is

$$T_{ol}(s) = \frac{Y(s)}{U(s)} = \frac{1}{s^2 + 2\zeta\omega_0 s + \omega_0^2} \tag{1}$$

where ζ is the damping factor and ω_0 is the resonance frequency in radian measure. The closed-loop transfer function is

$$T_{cl}(s) = \frac{T(s)}{1 + T(s)H(s)} \tag{2}$$

This is a second-order system and we will illustrate two control methodologies, proportional control and proportional/derivative control. In the first, the feedback is proportional to the output, *Y*, so that

$$H(s) = K_p \tag{3}$$

and

$$T_p(s) = \frac{1}{s^2 + 2\zeta\omega_0 s + (\omega_0^2 + K_p)} \tag{4}$$

Here, the effect of a positive K_p is primarily an increase in resonance frequency and a drop in overall gain. In the second system, a fraction of the output and a fraction of the derivative of the output are fed back to the input:

$$H(s) = K_p + K_d s \tag{5}$$

and

$$T_{pd}(s) = \frac{1}{s^2 + (2\zeta\omega_0 + K_d)s + (\omega_0^2 + K_p)} \tag{6}$$

The principal effect of a positive K_d is an increase in damping. The effects of both types of control are illustrated in Fig. 2. For both control strategies, the system gain is reduced. The proportional/derivative strategy produces the flattest amplitude response.

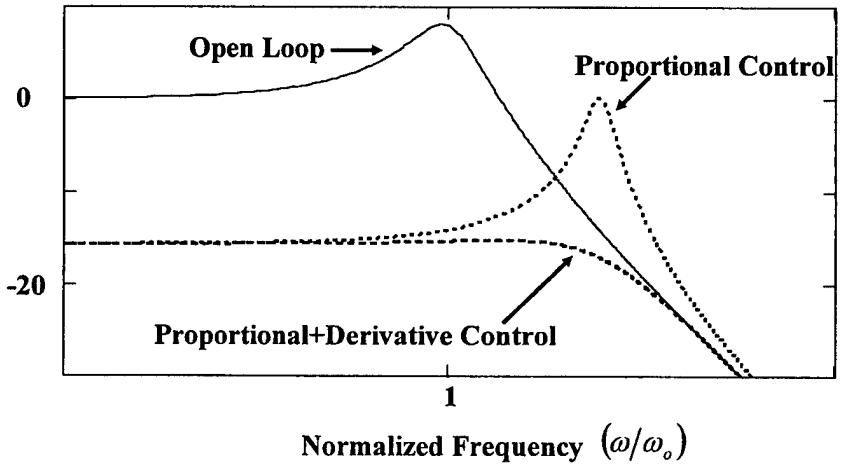

Figure 2. Performance of a simple, second-order system under both proportional and proportion/derivative control. For this example, the damping factor, ζ, was 0.2 and the control constants were $K_p = 5$ and $K_d = 2.5$. The vertical scale is in decibels and the horizontal scale is logarithmic.

For linear systems, classical control theory is well developed and powerful; however, for systems with substantial nonlinearity, other techniques are more valuable. One of those techniques is the method of state variables.

Introduction to the State-Variable Technique

Classical control theory focuses on linear systems and their frequency-domain characteristics. As the system size grows, the analysis complexity grows. Modern control theory is often based on state variables. In this technique, the system is treated in the time domain as a set of coupled

first-order differential equations. While less straightforward and less intuitive than the classical techniques, nonlinear elements are not intrinsically problematic. In addition, representation in terms of a coupled set of first-order equations facilitates analysis using power linear-algebra methods. A multiple-input/multiple-output system has the same basic representation as a single-input/single-output system. The increase in "complexity" is merely an increase in matrix dimension (and, of course, in computer run time).

The second-order system considered in the classical analysis above has the following time-domain representation:

$$\ddot{y} = -\omega_0^2 y - 2\zeta\omega_0 \dot{y} + u \tag{7}$$

where the lower-case letters indicate that these functions are functions of time and the dots indicate derivatives with respect to time. In state-variable notation, a vector, **x**, is created from the system displacement and the system velocity:

$$\mathbf{x} = \begin{bmatrix} displacement \\ velocity \end{bmatrix} = \begin{bmatrix} y \\ \dot{y} \end{bmatrix} \tag{8}$$

The second-order differential equation can be written as a matrix equation in terms of two first-order equations:

$$\dot{\mathbf{x}} = \begin{bmatrix} 0 & 1 \\ -\omega_0^2 & -2\zeta\omega_0 \end{bmatrix} \mathbf{x} + \begin{bmatrix} 0 \\ 1 \end{bmatrix} u \tag{9}$$

or

$$\dot{\mathbf{x}} = \mathbf{A}\mathbf{x} + \mathbf{B}u \tag{10}$$

In the classical analysis, the behavior of the solution is controlled by the poles of the denominator of the transfer function,

$$s^2 + 2\zeta\omega_0 s + \omega_0^2 = 0 \tag{11}$$

In state-variable analysis, the behavior of the solution is controlled by the eigenvalues (and eigenvectors) of the matrix equation,

$$|\mathbf{A} - \lambda\mathbf{I}| = \lambda^2 + 2\zeta\omega_0\lambda + \omega_0^2 = 0 \tag{12}$$

For this simple example, the solutions are identical (with $s = \lambda$) as they should be. For more complex examples, the matrix equation in the state-variable approach expands in dimension and the elements can be nonlinear, but the form remains the same and the solution is still an eigenvalue problem.

General Sensor Model

The target sensor design is a differential-capacitance accelerometer with electrostatic-force feedback (see Fig. 3). The electrostatic force feedback is nonlinear. In addition, because of fringing fields, the sense mechanism is nonlinear. Furthermore, the flexure may be nonlinear for large deflection.

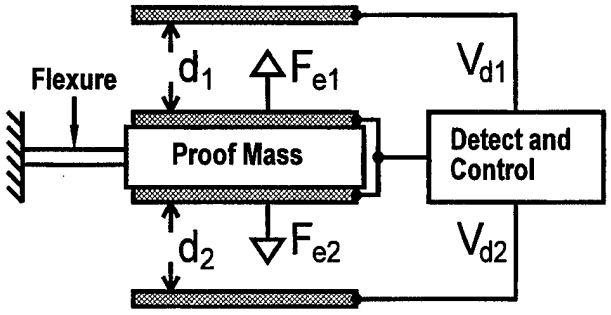

Figure 3. General model of differential-capacitance accelerometer with electrostatic force feedback. Although sense and actuation are shown to use the same electrodes, in practice, the electrodes may be separate. This introduces no fundamental problem in the analysis.

The mechanical model used here represents the mass and stiffnesses as equivalent lumped-element parameters. For an edge-hinged proof mass, the dynamic mass is not the same as the mass of the moving element itself and similar considerations extend to the stiffness of the flexure especially in the vicinity of resonance. Modes of vibration higher than the fundamental will be ignored; however, both damping and electrostatic forces will be permitted to be nonlinear. If the damping is fluid dynamic, then the damping force is only directly proportional to the proof-mass velocity over a relatively small range of physical parameters. The mechanical model is shown in Fig. 4.

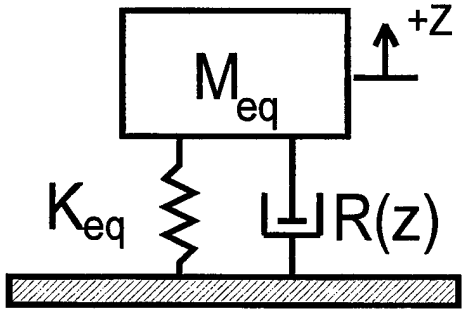

Figure 4. Mechanical model for mechanism. The electrostatic actuation force is not shown but the potentially nonlinear damping, *R(z)*, is shown.

The electrical model (Fig. 5) is based on a differential-capacitance configuration. Two outer, fixed plates are driven by 0° and 180° phase sine waves and the moveable center plate produces an output consisting of an amplitude modulated carrier. For the purposes of this analysis, the moving plate will be considered parallel to the fixed plates for all deflections. In the case in which the moving plate is hinged on one side, this is not true but the moving plate can also be suspended with flexures on both sides to maintain parallelism.

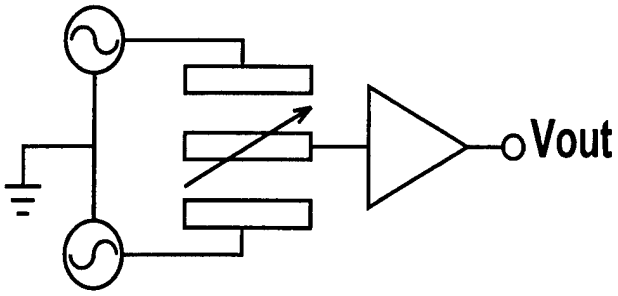

Figure 5. Electrical model for mechanism. The signal on the moving plate is a sine wave with the same frequency as the drive. The amplitude is directly proportional to the offset of the plate with respect to center (neglecting fringing effects).

State-Variable Representation

The dynamical equation for the sensor model outlined above is

$$ma = m\ddot{z} + R\dot{z} + kz + F_{e1} - F_{e2} \tag{13}$$

where a is the external acceleration and F_{e1} and F_{e2} are the actuation forces applied by the fixed plates. The damping is taken to be squeeze-film damping between the moving plate and both fixed plates:

$$R = \frac{3\mu A^2}{2\pi}\left[\frac{1}{(d_1 - z)^3} + \frac{1}{(d_2 - z)^3}\right] \tag{14}$$

and the electrostatic actuation force from one fixed plate is

$$F_{e1} = -\frac{\varepsilon_0 A}{2(d_1 - z)^2} V_{d1}^2 \tag{15}$$

with an identical expression for the other fixed plate. In these expressions, d_1 and d_2 are the equilibrium distances from the moving plate to either fixed plate, z is the displacement of the

moving plate from equilibrium, A is the electrode surface area, V_d is the voltage on the fixed plate, and μ is the viscosity of the gas between the plates.

The basic dynamical equation can be solved for the acceleration of the proof mass:

$$\ddot{z} = -\omega_0^2 z - \frac{R}{m}\dot{z} - \frac{1}{m}(F_{e1} - F_{e2}) + a \tag{16}$$

The state variables are

$$\mathbf{x} = \begin{bmatrix} \textit{displacement} \\ \textit{velocity} \\ \textit{top - plate voltage} \\ \textit{bottom - plate voltage} \end{bmatrix} = \begin{bmatrix} x_1 \\ x_2 \\ x_3 \\ x_4 \end{bmatrix} = \begin{bmatrix} z \\ \dot{z} \\ V_{d1} \\ V_{d2} \end{bmatrix} \tag{17}$$

and the system inputs are

$$\mathbf{u} = \begin{bmatrix} \textit{top control voltage} \\ \textit{bottom control voltage} \\ \textit{inertial acceleration} \end{bmatrix} = \begin{bmatrix} u_1 \\ u_2 \\ u_3 \end{bmatrix} = \begin{bmatrix} V_{d1} \\ V_{d2} \\ a \end{bmatrix} \tag{18}$$

The state functions are

$$\dot{z} = \dot{x}_1 = f_1(x,u) \tag{19}$$

$$\ddot{z} = \dot{x}_2 = f_2(x,u) \tag{20}$$

$$\dot{V}_{d1} = \dot{x}_3 = f_3(x,u) \tag{21}$$

$$\dot{V}_{d2} = \dot{x}_4 = f_4(x,u) \tag{22}$$

and the system output is

$$V_{out} = y = g(x,u) \tag{23}$$

Small-Signal Analysis

Once the state-variable formulation has been constructed, the solution for small amplitudes can be derived. This permits a direct check against classical, linearizing techniques. First, the static equilibrium points are located:

$$f(x_e, u_0) = 0 \tag{24}$$

Then we consider small perturbations about the equilibrium state:

$$x = x_e + \delta x \tag{25}$$

$$u = u_0 + \delta u \tag{26}$$

$$y = g(x_e, u) \tag{27}$$

and

$$\dot{x} = \delta\dot{x} = \mathbf{f}(x, u) \tag{28}$$

Next, the state functions are expanded as Taylor series and only the first-order terms are retained:

$$\mathbf{f}(x, u) \approx \mathbf{A}\delta x + \mathbf{B}\delta u \tag{29}$$

and similarly for the system-output g functions so that

$$\mathbf{A} = \nabla_x f_e \;;\; \mathbf{B} = \nabla_u f_e \;;\; \mathbf{C} = \nabla_x g_e \;;\; \mathbf{D} = \nabla_u g_e \tag{30}$$

The small signal model is then,

$$\delta\dot{x} = \mathbf{A}\delta x + \mathbf{B}\delta u \quad ; \quad \delta y = \mathbf{C}\delta x + \mathbf{D}\delta u \tag{31}$$

Example of State-Variable Analysis

As an example of this analysis, dimensions of a prototype accelerometer were used and the full, nonlinear analysis was performed. The plate area, A, was 2 mm^2, the equilibrium plate gap, d_0, was 20 μm, the proof mass, m, was 2.6 mg, and the stiffness, k_{eq}, was 13.4 N/m. These parameters produced a resonance frequency, ω_0, of 2277 radians/sec and a damping factor, ζ, of 0.726 (which corresponds to a Q of 0.688).

The results of the nonlinear model are shown in Fig. 6. As the excitation acceleration increases, the waveform distortion grows, as does harmonic generation.

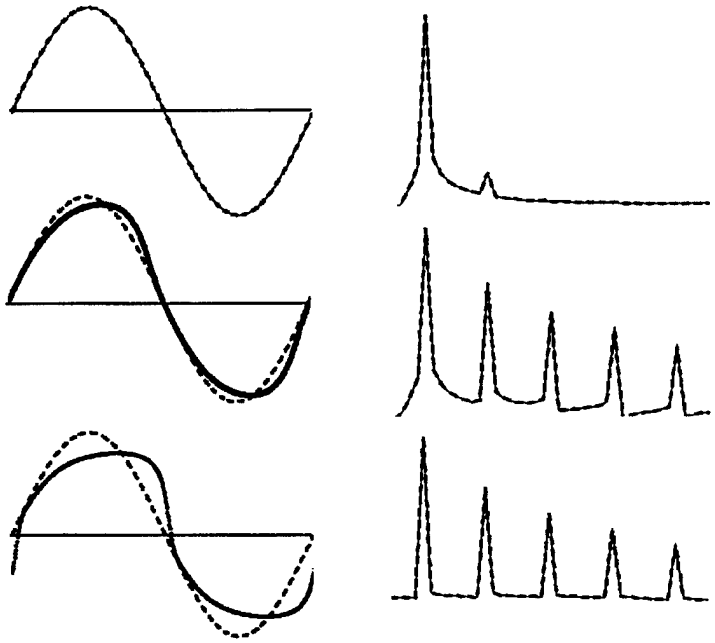

Figure 6. State-variable simulation of open-loop performance of accelerometer. The time series output (for sinusoidal input) is shown in the left column and the frequency-domain output is shown in the right column. From the top down, the input accelerations are 1g, 7g, and 10g. At 10g, the motion of the proof mass is almost all the way from fixed plate to fixed plate. Since the distortion is symmetric, only odd harmonics appear. From top to bottom, the amplitude ratio of the third harmonic to the first is -57 dB, -21 dB, and -14 dB.

Summary

A state-variable analysis has been implemented for the nonlinear, closed-loop accelerometer. Nonlinearities in electrostatic actuation and in gas-dynamic damping have been considered. The small signal (linear) behavior has been obtained and the nonlinear open-loop response has been modeled. This tool should prove useful in designing closed-loop sensors particularly with respect to instabilities that are directly associated with large-amplitude behavior.

LABORATORY EXPERIMENTS

1. Basic Noise Measurement

Objectives

- Measure Johnson noise of a resistor
- Measure equivalent input current and voltage noise of several op amps
- Examine excess noise produced by current forced through resistance

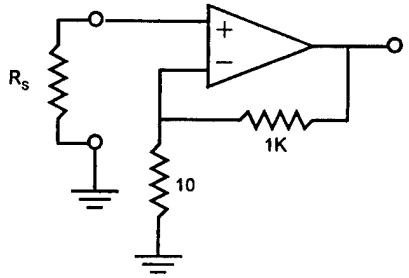

Figure 1.1. Basic circuit for noise measurement. An operational amplifier is configured for a voltage gain of 100. The gain-setting resistors are selected so that their Johnson noise does not contribute significantly to the overall noise. Various resistors are connected to the + input and the output noise is measured using a spectrum analyzer.

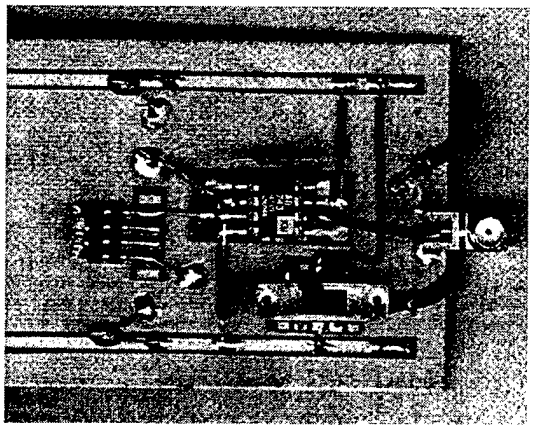

Figure 1.2. Circuit layout. Socket permits evaluation of any standard 8-pin operational amplifier. Resistors are inserted using single-in-line connector on left. Circuit is built on a copper ground plane and battery powered to minimize 60 Hz interference. No other shielding is necessary.

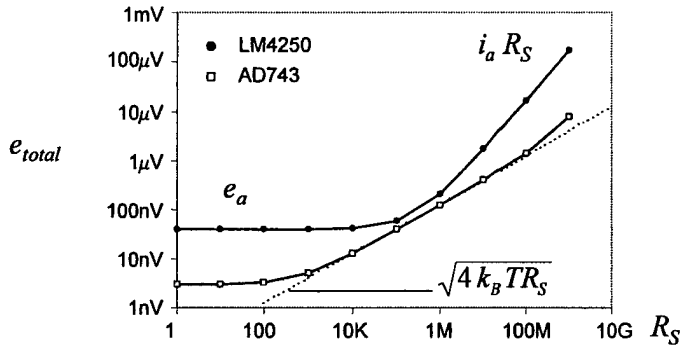

Figure 1.3. Typical measurement results from circuit in Fig. 1.2. Upper curve is for a micropower LM4250 with relatively high noise; lower curve is for the low-noise AD743. The dotted curve is the Johnson noise from the test resistor. The AD743 is able to measure the resistor's Johnson noise over a wide range of resistance, whereas the LM4250 internal noise always dominates. For low resistance, the amplifier's equivalent voltage noise, e_a, dominates. For high resistance, the amplifier's equivalent current noise flowing into the resistance, $i_a R_S$, dominates.

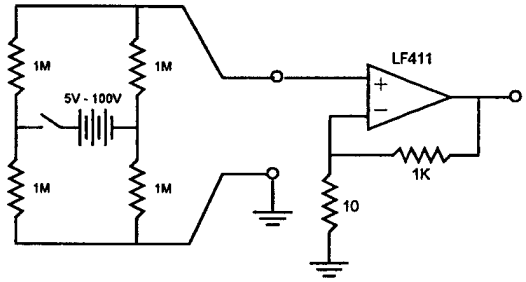

Figure 1.4. Circuit for measurement of excess noise resulting from current flow through a resistor. The circuit of Fig. 1.1 is modified so that a bridge of resistors and a voltage source can be connected to the + input. The bridge configuration permits application of the external voltage without changing the DC conditions at the + input.

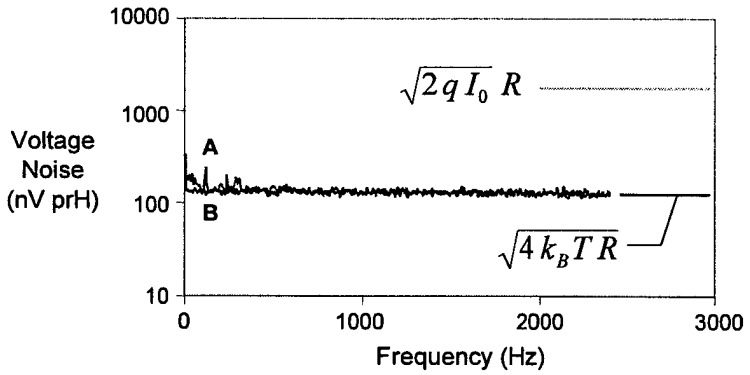

Figure 1.5. Results of noise measurement with (A) and without (B) current through resistor bridge. If shot noise were produced, the level would be as shown by the upper straight-line segment. Over most of the frequency range, however, the noise is well represented by Johnson noise whether or not current is flowing. There is a small, additional low-frequency noise component when current is flowing. Its power spectrum is inversely proportional to frequency ("1/f" noise).

2. Measuring Noise Performance of a Low-Noise Bipolar Transistor Amplifier

Objectives

- Measurement of equivalent voltage and current noise for a bipolar transistor
- Measure base leakage current and relate to shot noise
- Experiment with offset correction
- Demonstrate achieved noise below 2 nanovolts per root hertz

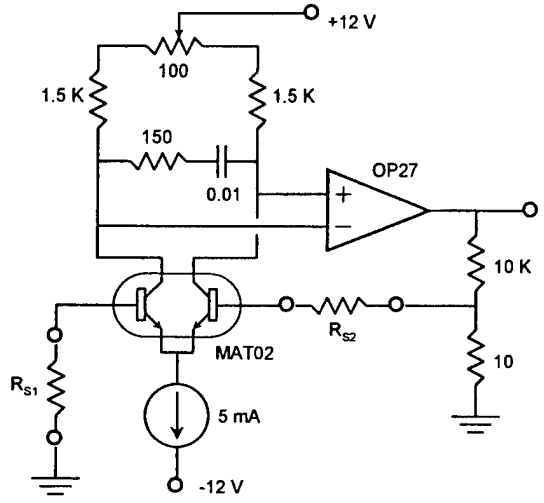

Figure 2.1. Circuit for noise measurement of bipolar junction transistor. Bipolar transistors are excellent for low voltage noise but they are also accompanied by high leakage currents from the base. This circuit permits balancing of the voltage produced by the leakage and also permits measuring the leakage so the shot-noise component can be calculated and compared to the measurement. With R_{S2} set to zero, the DC output is the leakage current times R_{S1} times the voltage gain of the circuit (x100). This permits calculation of the current shot noise. Measurement of the current noise requires large values for R_{S1} but the leakage current can produce enough of a DC offset that the amplifier saturates. Setting R_{S2} equal to R_{S1} permits balancing of the offset. The resulting noise power is twice that from one resistor.

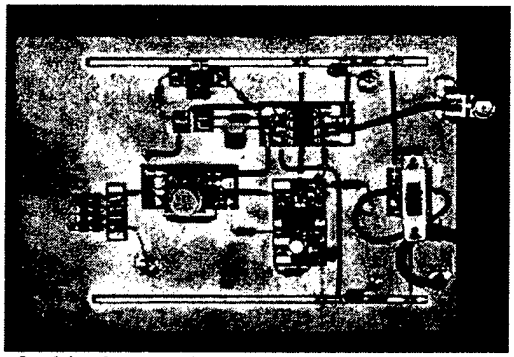

Figure 2.2. Circuit layout for bipolar transistor noise measurement. The circuit is constructed on a copper ground plane and battery powered for immunity from 60 Hz interference. Both R_{S1} and R_{S2} are plug-in components.

3. AC-Drive of Bridge Sensors

Objectives

- Compare DC and AC performance of strain-gage bridge
- Calibrate strain response for static and dynamic deflection
- Examine phase-synchronous detection process
- Measure resistance to external electromagnetic interference

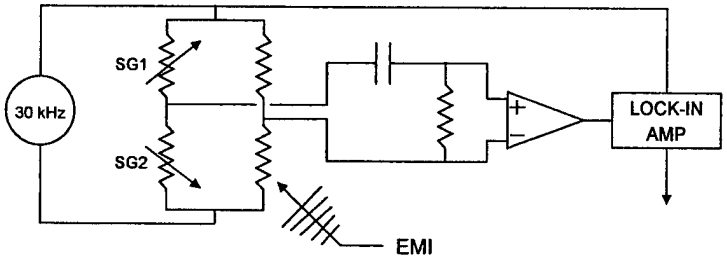

Figure 3.1. Circuit for AC-drive of bridge sensors. A strain-gage bridge is driven by either DC or high-frequency AC. With DC drive, the bridge output is measured directly. There is very little immunity to external interference. With AC drive, the bridge output is high-pass filtered, amplified, and detected synchronously using a lock-in amplifier. The immunity to external interference is very high.

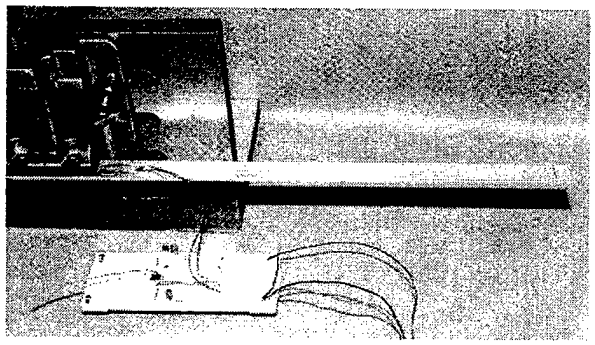

Figure 3.2. Physical set up. Two strain gages are attached to an aluminum bar. The aluminum bar is clamped near the strain gages so that it forms a cantilever beam. The bridge is completed by matched resistors on the breadboard. High levels of external interference are introduced by placing the ballast transformer from a fluorescent light next to the wires from the strain gages. Static deflection is produced by placing a weight on the free end of the cantilever. The strain gage response can be checked against the theoretical strain produced by the end loading. Dynamic response is examined by striking the beam to excite various resonances.

4. Differential-Capacitance Displacement Sensor

Objectives

- Build a differential-capacitance displacement sensor
- Build drive and detection electronics
- Perform an absolute calibration of displacement response
- Measure beam vibration amplitude

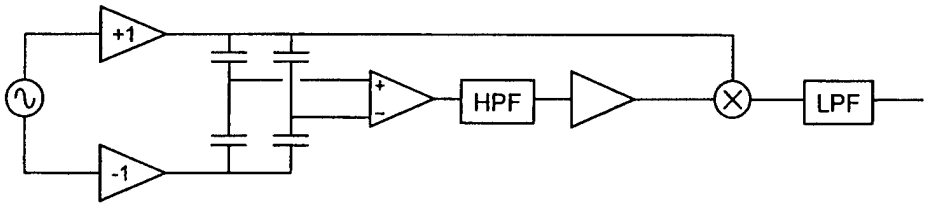

Figure 4.1. Circuit for the differential-capacitance sensor. The circuit show above is for a full bridge sensor; however, a half-bridge set up is used in the laboratory. The differential capacitor is driven by 0° and 180° phases of a high-frequency sine wave. The bridge output is high-pass filtered (HPF), amplified, and detected synchronously with the excitation by analog multiplication (X) and low-pass filtering (LPF).

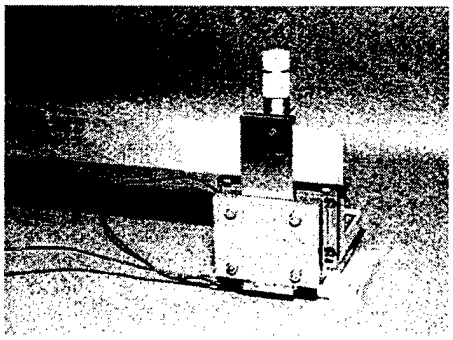

Figure 4.2. Physical set up of differential-capacitance element. An aluminum beam is clamped at one end. The clamp is to the left out of the field of the picture. A fixture holds two brass plates on a micrometer translation stage. The brass plates are spaced slightly wider than the beam is thick. The translation stage permits centering of the plates with respect to the beam and permits absolute displacement calibration. Once the static response is determined by the displacement calibration, dynamic measurement of beam resonances is performed.

5. Closed-Loop Control of Inverted Pendulum

Objectives

- Examine instability of inverted pendulum
- Measure loop gain of simple feedback control loop
- Construct differential-capacitance displacement sensor
- Construct constant-force rebalance actuator
- Examine control-loop instability and lead-lag compensation

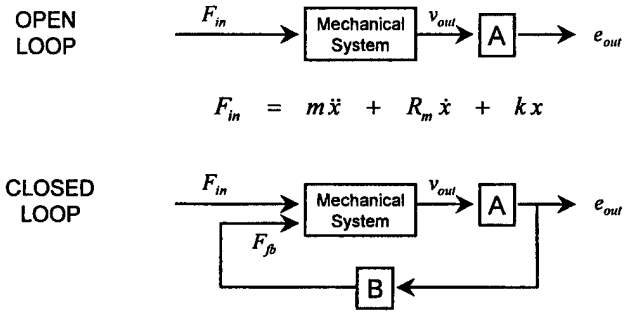

Figure 5.1. Comparison of open-loop and closed-loop mechanical systems. The simple damped mass-spring system translates an applied force to some velocity of the moving mass. The transducer translates that velocity into a voltage. In the closed-loop system, that voltage is translated (by the control transducer) into a force and applied to the mass. For this case, the force is proportional to the velocity so the feedback either increases or decreases the damping.

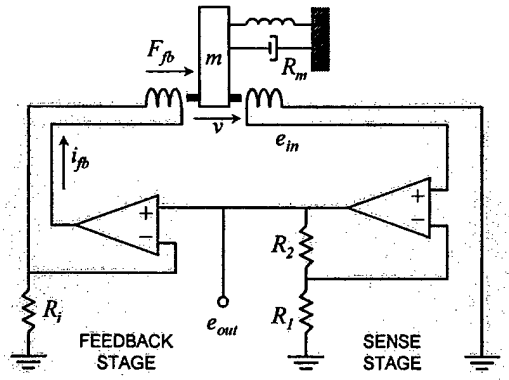

Figure 5.2. Schematic diagram of the feedback apparatus. In this representation, both the sense and control transducers are electrodynamic. A magnet on the moving mass moves into and out of a fixed coil. The voltage generated is proportional to the velocity of the mass. For closed-loop operation, that voltage is converted to a current in the feedback stage and applied to another coil in proximity with another magnet on the moving mass. The applied force is proportional to the current in the coil. By reversing the connections on either coil, the feedback damping can be changed from positive resistance to negative resistance. Application of sufficient negative resistance causes the system to oscillate.

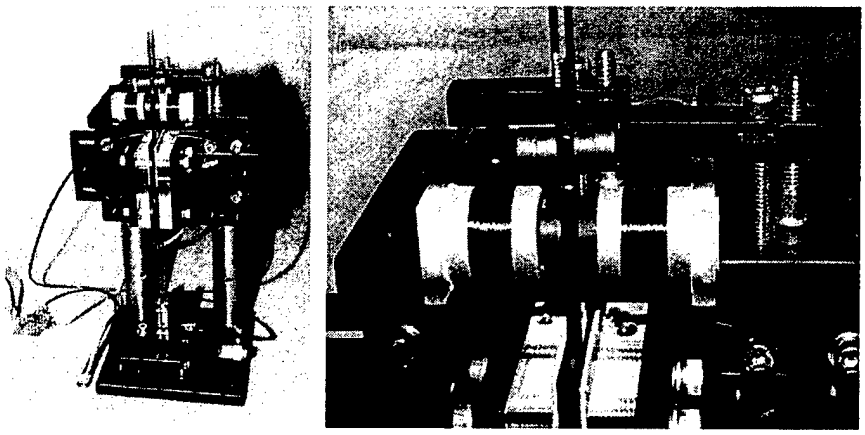

Figure 5.3. Laboratory apparatus for feedback control of an inverted strut. The entire assembly is shown on the left and a close-up view of the control actuator is shown on the right. In this version, the sensing is done with a differential-capacitance displacement sensor so the sensed voltage is proportional to displacement, not velocity. The control transducer is electrodynamic and is drive by a voltage-to-current converter. In this case, the feedback force is proportional to displacement so it represents a strengthening or weakening of the stiffness. Additional magnets added above the drive coils (see right side) can cause the strut to collapse but addition of feedback stiffness restores the stability of the strut. The control circuitry requires a small amount of lead compensation to make the system stable. This compensation corrects for the non-ideal phase shifts introduced by the electrical components.

REFERENCES

[1] J. G. Simmons, "Generalized formula for the electric tunnel effect between similar electrodes separated by a thin insulating film," J. Appl. Phys. **34**, 1793-1803, 1963.

[2] D. P. DiLella, J. H. Wandass, R. J. Colton, C. R. K. Marrian, "Control systems for scanning tunneling microscopes with tube scanners," Rev. Sci. Instrum. **60**, 997-1002, 1989.

[3] T. W. Kenny, W. J. Kaiser, H. K. Rockstad, J. K. Reynolds, J. A. Podesek, and E. C. Vote, "Wide-bandwidth electromechanical actuators for tunneling displacement transducers," J. Microelectromechanical Systems **3**, 97-104, 1994.

[4] D. W. Pohl, "Some design criteria in scanning tunneling microscopy," IBM J. Res. Develop. **30**, 417-427, 1986.

[5] A. B. Pippard, *Response and Stability*, Cambridge University Press, NY, 1985.

[6] J. Schwarzenbach and K. F. Gill, *System Modelling and Control*, Halsted Press, NY, 1992.

[7] MatLab and Simulink are products of The MathWorks, Inc., 24 Prime Park Way, Natick, MA 01760-9889. Various products are mentioned in this report but such mention should not be construed to be endorsement or recommendation.

[8] This section is based on the paper, B. Doust, T. Gabrielson, and J. Schiano, "Generalized state-variable model for the design of a closed-loop differential accelerometer," presented at the Acoustical Society of America (Columbus, Ohio meeting), November 4, 1999.